AD-A134 743 ATMOSPHERIC SCINTILLATION AT 94 GHZ(U) ARMY MISSILE 1/1
COMMAND REDSTONE ARSENAL AL ADVANCED SENSORS
DIRECTORATE P M ALEXANDER ET AL. 01 DEC 82
UNCLASSIFIED DRSMI-RE-83-16-TR SBI-AD-E950 457 F/G 17/9 NL

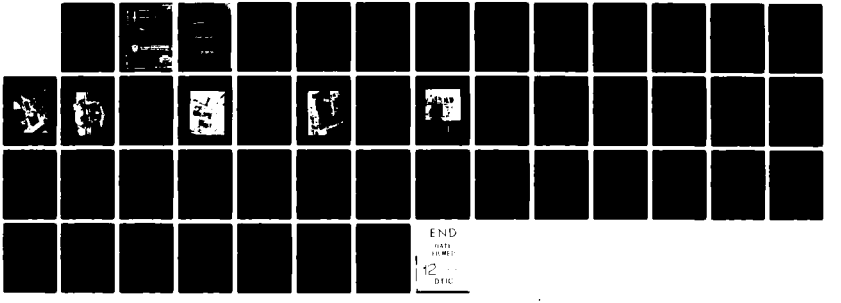

END
DATE FILMED
12
DTIC

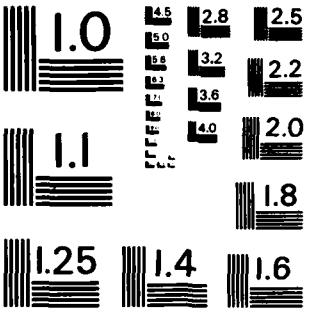

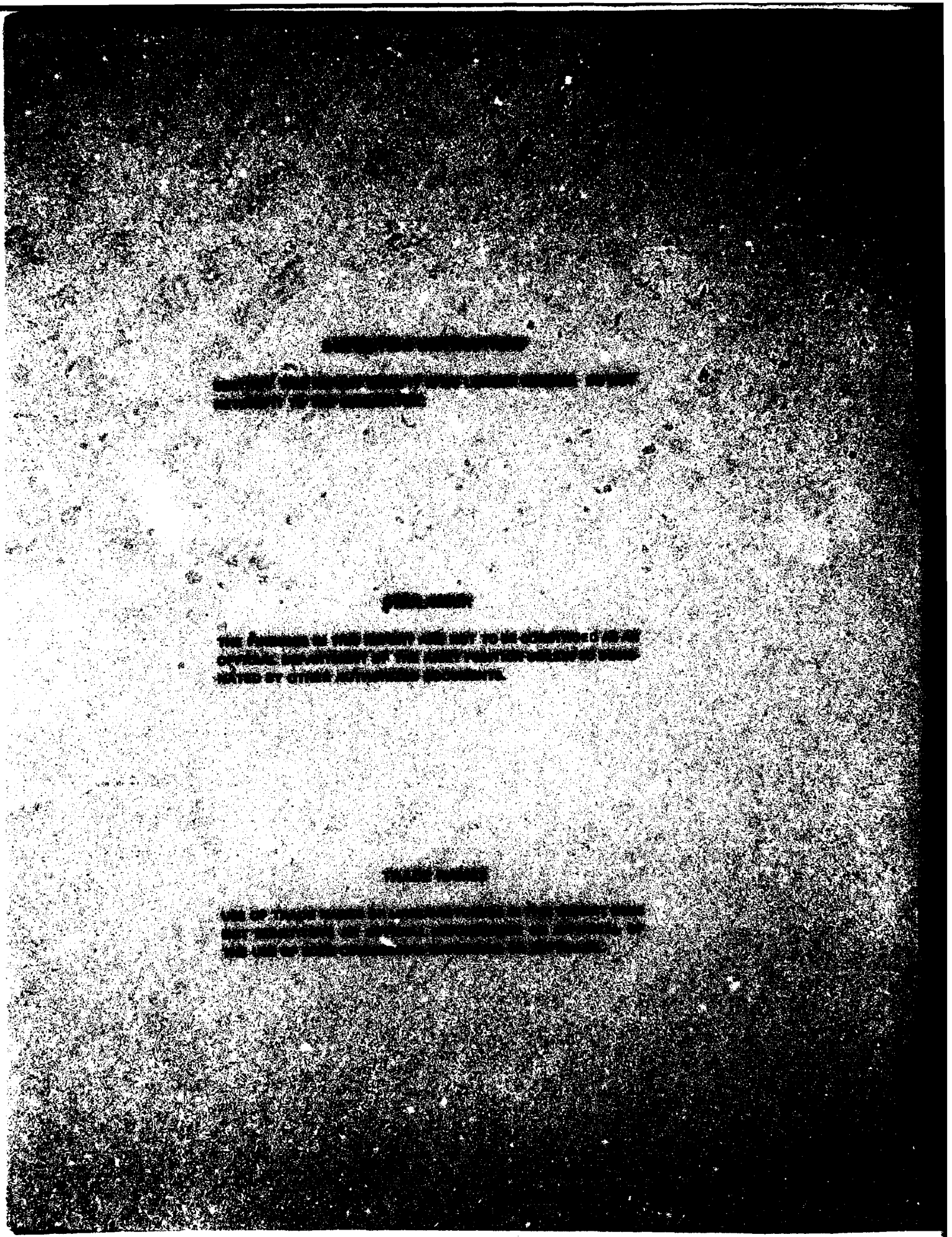

UNCLASSIFIED

SECURITY CLASSIFICATION OF THIS PAGE (When Data Entered)

REPORT DOCUMENTATION PAGE		READ INSTRUCTIONS BEFORE COMPLETING FORM
1. REPORT NUMBER TR-RE-83-16	2. GOVT ACCESSION NO. AD-A134 193	3. RECIPIENT'S CATALOG NUMBER
4. TITLE (and Subtitle) Atmospheric Scintillation at 94 GHz		5. TYPE OF REPORT & PERIOD COVERED Technical Report 6. PERFORMING ORG. REPORT NUMBER
7. AUTHOR(s) P. M. Alexander H. M. Grass		8. CONTRACT OR GRANT NUMBER(s)
9. PERFORMING ORGANIZATION NAME AND ADDRESS Commander, US Army Missile Command ATTN: DRSMI-REL Redstone Arsenal, AL 35898		10. PROGRAM ELEMENT, PROJECT, TASK AREA & WORK UNIT NUMBERS
11. CONTROLLING OFFICE NAME AND ADDRESS Commander, US Army Missile Command ATTN: DRSMI-RE Redstone Arsenal, AL 35898		12. REPORT DATE 1 December 1982 13. NUMBER OF PAGES
14. MONITORING AGENCY NAME & ADDRESS(if different from Controlling Office)		15. SECURITY CLASS. (of this report) UNCLASSIFIED 15a. DECLASSIFICATION/DOWNGRADING SCHEDULE

16. DISTRIBUTION STATEMENT (of this Report)

Cleared for public release; distribution unlimited.

17. DISTRIBUTION STATEMENT (of the abstract entered in Block 20, if different from Report)

18. SUPPLEMENTARY NOTES

19. KEY WORDS (Continue on reverse side if necessary and identify by block number)

Millimeter Waves
W Band
Atmospheric Turbulence
Atmospheric Scintillation
Radar

20. ABSTRACT (Continue on reverse side if necessary and identify by block number)

An experimental 94 GHz transmitter and receiver were developed for measuring amplitude fluctuations due to clear-air turbulence. Atmospheric scintillation theory is discussed, and experimental conditions are described. Atmospheric fluctuations could not be observed above the transmitter/receiver noise, thus establishing an estimated upper bound that was about a factor of ten lower than fluctuations predicted from optical theory.

DD FORM 1 JAN 73 1473 EDITION OF 1 NOV 65 IS OBSOLETE

UNCLASSIFIED

SECURITY CLASSIFICATION OF THIS PAGE (When Data Entered)

ACKNOWLEDGMENT

The funding for this research was provided by the US Army Missile Labortory's In-house Laboratory Independent Research (ILIR) program, fund number 725 T01-49-00.

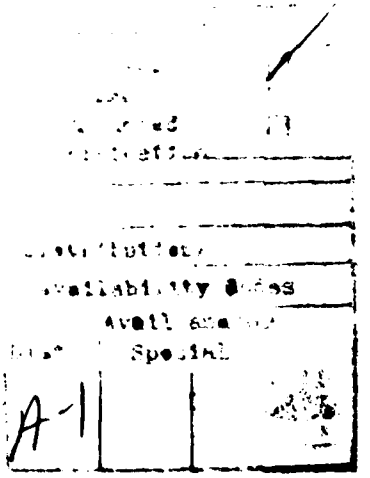

CONTENTS

I. INTRODUCTION

The purpose of this experimental effort was to study the effects of clear-air turbulence in millimeter-wave radar systems. The desired end result is a measure of angle-tracking errors resulting from angle-of-arrival fluctuations of the radar beam. The application of this work is directed toward a surface-to-surface, direct-fire, anti-tank missile using millimeter-wave beamrider or differential guidance. The measurement of atmospheric scintillation at 94 GHz is a first step towards determining angle-of-arrival fluctuations.

Initially, it was noted that, with a single receiving antenna, amplitude fluctuations cannot be distinguished from apparent amplitude variations due to angle-of-arrival fluctuations. However, expected angle-of-arrival fluctuations are on the order of 0.02° peak-to-peak (see Section IV), while the 3 dB beamwidth of the receiving antenna is 0.70°. Thus, angle-of-arrival effects are small compared to expected amplitude fluctuations of ~ 1 dB (~ 25%).

The experimental work was carried out under worst-case conditions, i.e., over an asphalt road with temperatures in the eighties and relative humidities from 60% to 70%. Mirages, mirror-like images of the sky reflected from air in contact with the ground, were highly visible. These reflections are the result of a lower refractive index, due to expansion of the air, and total internal reflection. The laser system used also indicated a high degree of atmospheric turbulence.

Section II discusses the theory used to describe atmospheric scintillation, while Section III describes the experimental apparatus. In Section IV, experimental results are described and analyzed with respect to the theory of Section II. Conclusions are presented in Section V.

II. ATMOSPHERIC SCINTILLATION THEORY

The theory of atmospheric scintillation used to analyze experimental results is taken largely from the initial work done by Tatarski [1] and two review papers: Lawrence and Strohbein [2] and Fante [3]. Scintillation is defined as the time variation of the intensity (or power) of a received electromagnetic wave due to propagation through a randomly fluctuating medium.

At optical wavelengths, it is believed that scintillation results from variations of the index of refraction due to random temperature fluctuations. Effects of pressure variations are small. These temperature fluctuations, called "turbulent eddies", are thought of as pockets or bubbles of air having different temperatures than the surrounding atmosphere, and are characterized by a dimension or correlation distance called the "scale size". The strongest turbulent eddies are generated near the ground in direct sunlight, similar to bubbles forming at the bottom of a heated pan of water.

Because millimeter waves are absorbed by water vapor, scintillation at these wavelengths may also be due to humidity fluctuations along the propagation path [4,5]. Humidity fluctuations may cause index of refraction fluctuations as well as absorption variations.

The magnitude of index of refraction fluctuation is described by the quantity C_n^2, the index of refraction structure parameter, sometimes optimistically called the structure constant. In this work, the structure parameter is determined from experimentally measurable quantities using Equation [6] for a plane wave,

$$\sigma_\chi^2 = 0.31 \; C_n^2 \kappa^{7/6} R^{11/6} \quad , \qquad (1)$$

where σ_χ^2 is the variance of the log-amplitude χ, κ is the wavenumber (2π divided by the transmitted wavelength λ), and R is the path length or range. The log-amplitude is given by

$$\chi(t) = \ln \left[\frac{E(t)}{Eo}\right] \quad , \qquad (2)$$

where E(t) is the amplitude of the electric field at time t, and E_o is the time-averaged electric-field amplitude.

Since the received power p(t) (or intensity or irradiance for optical workers) is proportional to $E^2(t)$, the variance of the log-power (which is experimentally measured) is four times the (theoretically calculated) log-amplitude variance:

$$\sigma_{lnp}^2 = 4 \; \sigma_\chi^2 \quad , \qquad (3)$$

where the variances are defined by

$$\sigma_\chi^2 \triangleq \left\langle \ln^2 \left[\frac{E(t)}{Eo}\right] \right\rangle \qquad (4)$$

and

$$\sigma_{lnp}^2 \triangleq \left\langle \ln^2 \left[\frac{p(t)}{p_o}\right] \right\rangle \quad , \qquad (5)$$

and are equivalent to the mean-square values of ln E(t) and ln p(t). Again, p_o is a time-averaged value.

The theory is developed in terms of log-amplitudes or log-intensities because these have been found to have normally distributed (Gaussian) probability density functions for weak fluctuations.

A number of assumptions are inherent in Equation (1); these deal with the first Fresnel-zone size $\sqrt{\lambda R}$, the inner scale of the turbulent eddies l_o, and the outer scale of the turbulent eddies, L_o. L_o and l_o are the largest and smallest scale sizes of the existing turbulent eddies. Heating of the earth's surface creates large scale turbulent eddies that are broken down and mixed by the wind. The inner scale is thought to be on the order of a few millimeters, while, close to the earth, the outer scale is taken to be about the height of the beam above the earth, with some estimates at 1/3 and 1/5 this value.

One assumption is that

$$l_o << \sqrt{\lambda R} << L_o \quad . \qquad (6)$$

According to Tatarski [7], the turbulent eddies with scale sizes on the order of $\sqrt{\lambda R}$ make the largest contribution to amplitude fluctuations; Equation (6) ensures that such eddies are present. In the experimental work reported here, the Fresnel-zone size was about 2 meters for the millimeter-wave system and about 1.4 cm for the laser system. Thus, the condition that $\sqrt{\lambda R} << L_o$ may not be satisfied for the millimeter-wave system.

A second assumption of the theory is that

$$\lambda << l_o \quad , \qquad (7)$$

which requires the scattering to be mainly in the forward direction, even for the smallest turbulent eddies. For millimeter waves, this condition may not be well satisfied, resulting in significant Bragg-like scattering out of the main beam [8].

The assumption that

$$R << l_o^4/\lambda^3 \qquad (8)$$

is also used in deriving Equation (1), and this too is clearly not satisfied for the millimeter-wave system, but is well satisfied for the laser system.

Finally, the theory assumes that the fluctuations are small, i.e., that [9]

$$\sigma_\chi^2 < 0.64 \quad . \qquad (9)$$

Both the laser and millimeter-wave experimental conditions satisifed this criterion.

III. ATMOSPHERIC SCINTILLATION EXPERIMENT

The atmospheric scintillation experiment was performed at the US Army Missile Command's Vehicle Test Track, Test Area #7. This facility is adjacent to the Redstone Arsenal Airport and runs north and south as shown on the map in Figure 1. The track is a flat asphalt road, bordered on either side by brush or test surfaces (rocks, bumps, etc.). The 94 GHz transmitter was located at the north end of the range adjacent to Building 4820. The receiver front end was located in the bay of the Millimeter Guidance field-test trailer which was adjacent to Building 4819. The distance between receiver and transmitter, measured with a laser range finder, was 1232 meters; both receiver and transmitter antenna centers were 1.1 meters above the ground. All measurement and recording instrumentation and receiver processing were located inside the trailer. The HeNe laser for measuring the atmospheric scintillation at optical wavelengths was placed directly beside the 94 GHz receiver, while the laser receiver (a space averaging anemometer) was placed on the edge of the roadway at exactly 300 meters north of the laser. The anemometer outputs were transmitted to the trailer via a long coaxial cable.

Alignment of both the 94 GHz test system and the optical atmospheric scintillation equipments, although straightforward, required two operators. Once both the 94 GHz transmitter and receiver were operating and stablized, the two antennas were crudely aimed at each other. Then each was in turn carefully adjusted in azimuth and elevation until a maximum signal was received. In order to aid the receiver operator, the display of the IF spectrum analyzer, which was being used to monitor signal level and waveform, was displayed on an X-Y monitor in the trailer bay.

Similarly, once the space averaging anemometer had been positioned, the laser was crudely pointed using a telescope, and then very accurately pointed by observing the laser-beam reflection in the receiver optics. The laser receiver was then adjusted in azimuth and elevation to maximize the received signal. This adjustment was very precise, since the optical system was very sensitive to angular alignment. The space averaging anemometer, model CA-9 (Campbell Scientific, Logan, Utah), is generally used to measure wind speed, but also has an output directly giving the log-amplitude standard deviation, σ_χ. The principles of operation of this device are described by R. S. Lawrence, et.al. (1972) [10].

The 94 GHz transmitter consisted of a continuous wave (cw) reflex klystron source coupled to the transmitting antenna with provision made for monitoring the output frequency and power. A schematic diagram of the transmitter is shown in Figure 2. Initially, the klystron was mechanically tuned for a maximum output power around the desired center frequency of 94.12 GHz; fine tuning was accomplished by adjusting the reflector voltage. The klystron had a nominal average power output of 100 milliwatts. The transmitting antenna was a 60 centimeter diameter Cassegrain which provided a nominal 3 dB beamwidth of 5.3 milliradians at the operating frequency. Energy coupled out of the transmission path was directed through a cavity-type wavemeter to a power meter detector head. This provided a means for both monitoring the output power and setting the frequency. Very fine tuning of the frequency was

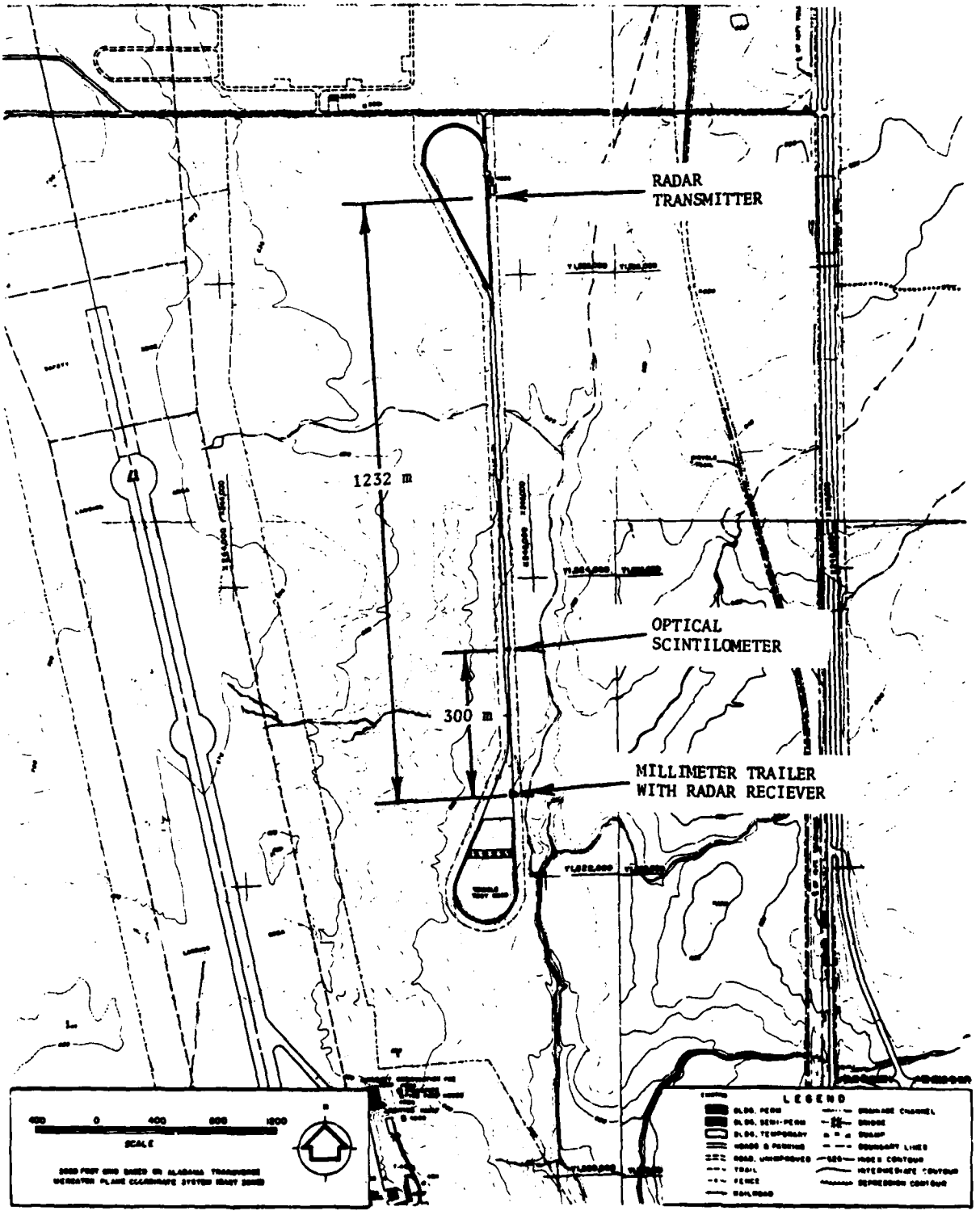

Figure 1. Vehicle test track, Test Area 7.

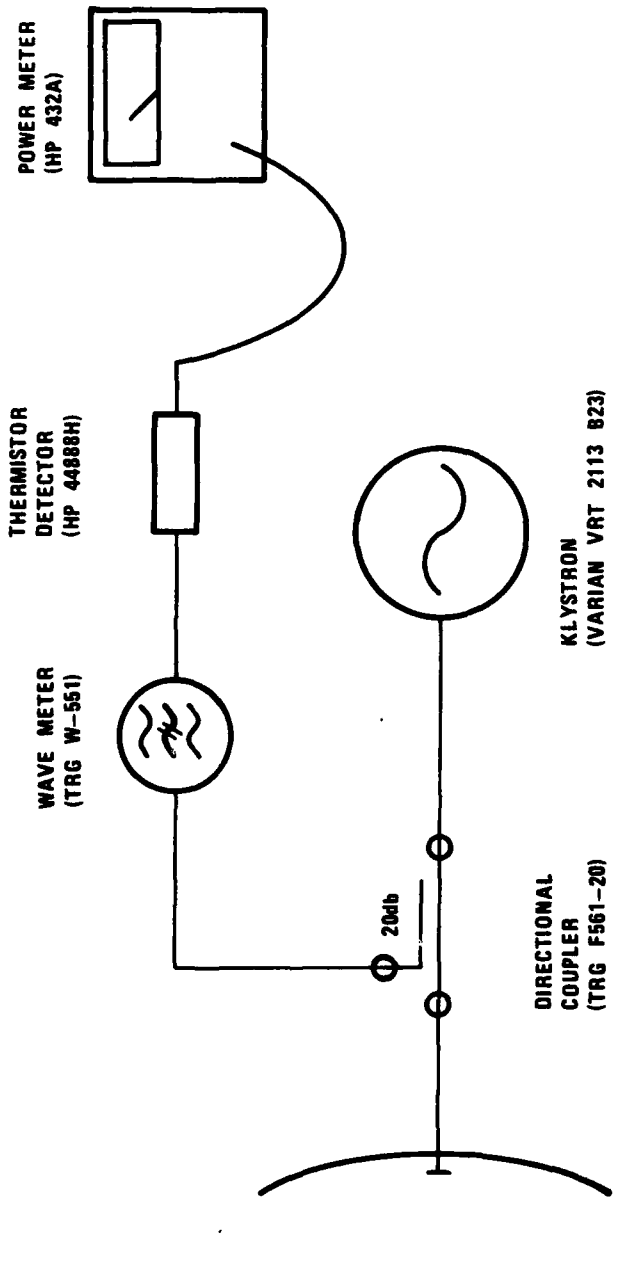

Figure 2. 94GHz transmitter schematic diagram.

accomplished by centering the frequency in the receiver passband. At one point, the thermistor head was replaced by a Schottky-diode detector for a measurement of long-term stability of the klystron. Figure 3 is a close-up photograph of the transmitter RF components in the normal operating configuration.

The transmitter components were installed in the eviscerated chassis of a spare brassboard radar. This was mounted on top of a standard cart which also held the Micro-Now klystron power supply and the klystron cooler. Flowing liquid coolant, a mixture of ethylene glycol and water, was used to stablized the operating temperature and minimize the effects of heating by the sun. Aiming the radar beam in azimuth was merely a matter of turning the cart; aiming in elevation was accomplished by blocking-up the rear of the radar chassis. Figure 4 is a photograph of the entire transmitter unit.

The 94 GHz receiver was physically and conceptually divided into two parts; i.e. the millimeter-wave portion and the intermediate frequency (IF) processing. The RF front-end was based upon the receiver section of a 94 GHz brassboard radar built by the Georgia Institute of Technology Engineering Experiment Station under contract DAAK40-78-C-0158. This provided a phase-locked Gunn-diode local oscillator whose frequency of 93.36 GHz established the operating frequency of the system. A high sensitivity mixer with built in preamplifier was used in place of the original mixer. In order to prevent damage to the mixer, a variable attenuator and power monitor were inserted ahead of the local oscillator. The receiving antenna was a Cassegrain with a 30 cm diameter main reflector, so that the receiving 3 dB beamwidth was approximately 10.5 milliradians. The output of the mixer preamplifier was directly coupled to an amplifier at the 750 MHz IF frequency.

The antenna, front-end, and power meter were mounted in a wooden box which was in turn mounted on an adjustable Hercules tripod. Aiming the receiver beam was straightforward, since the X-Y pan head of the tripod allowed the radar to be smoothly moved in azimuth and elevation; integral locks held the receiver position fixed once it had been aimed. Figure 5 is a schematic diagram of the entire receiver; the components comprising the front-end outside the trailer are inclosed within the dashed lines. Figure 6 is a top view of the front-end componentry. The unit at the right is the power meter for monitoring the local oscillator output, and the unit at the left is an auxilliary power supply.

The 750 MHz signal was delivered to the IF processing circuitry and recording instrumentation installed inside the trailer's equipment compartment via a 15 foot SMA cable. At this point the signal was passed through a variable attenuator and amplified, filtered, and split into two paths. The variable attenuator was used to set the signal at a fixed power, -10 dBm, using the spectrum analyzer, at the start of each test. The first signal path led to a second power splitter whose outputs were provided to an HP 8565A spectrum analyzer and a square-law detector. The spectrum analyzer served as the prime system monitor and performance analyzer. The negative output of the square-law detector was both displayed on an oscilloscope and amplified by a low-noise, wide bandwidth amplifier, PAR model 113, that also performed the signal inversion function.

Figure 3. 94 GHz transmitter components.

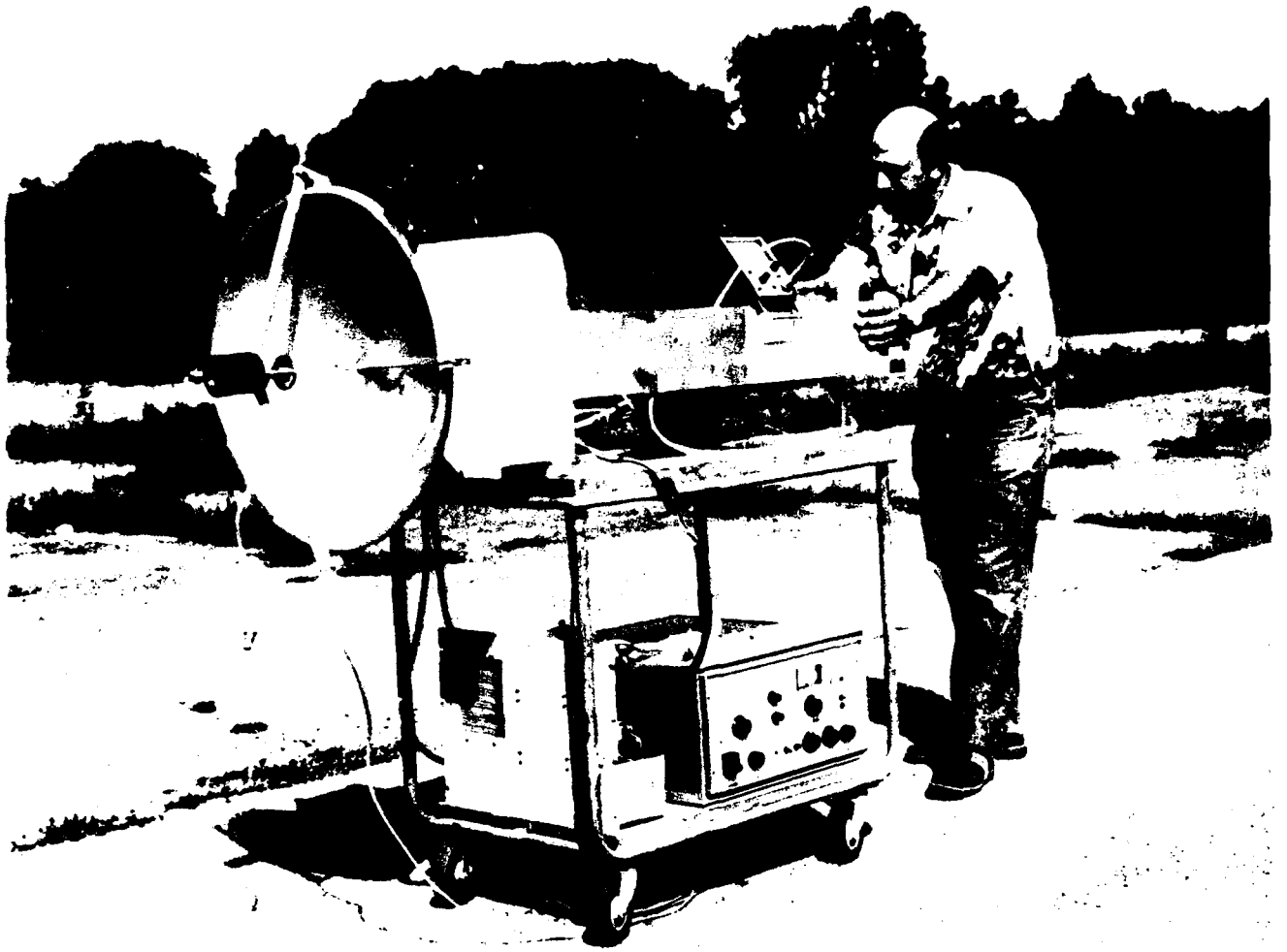

Figure 4. 94 GHz transmitter.

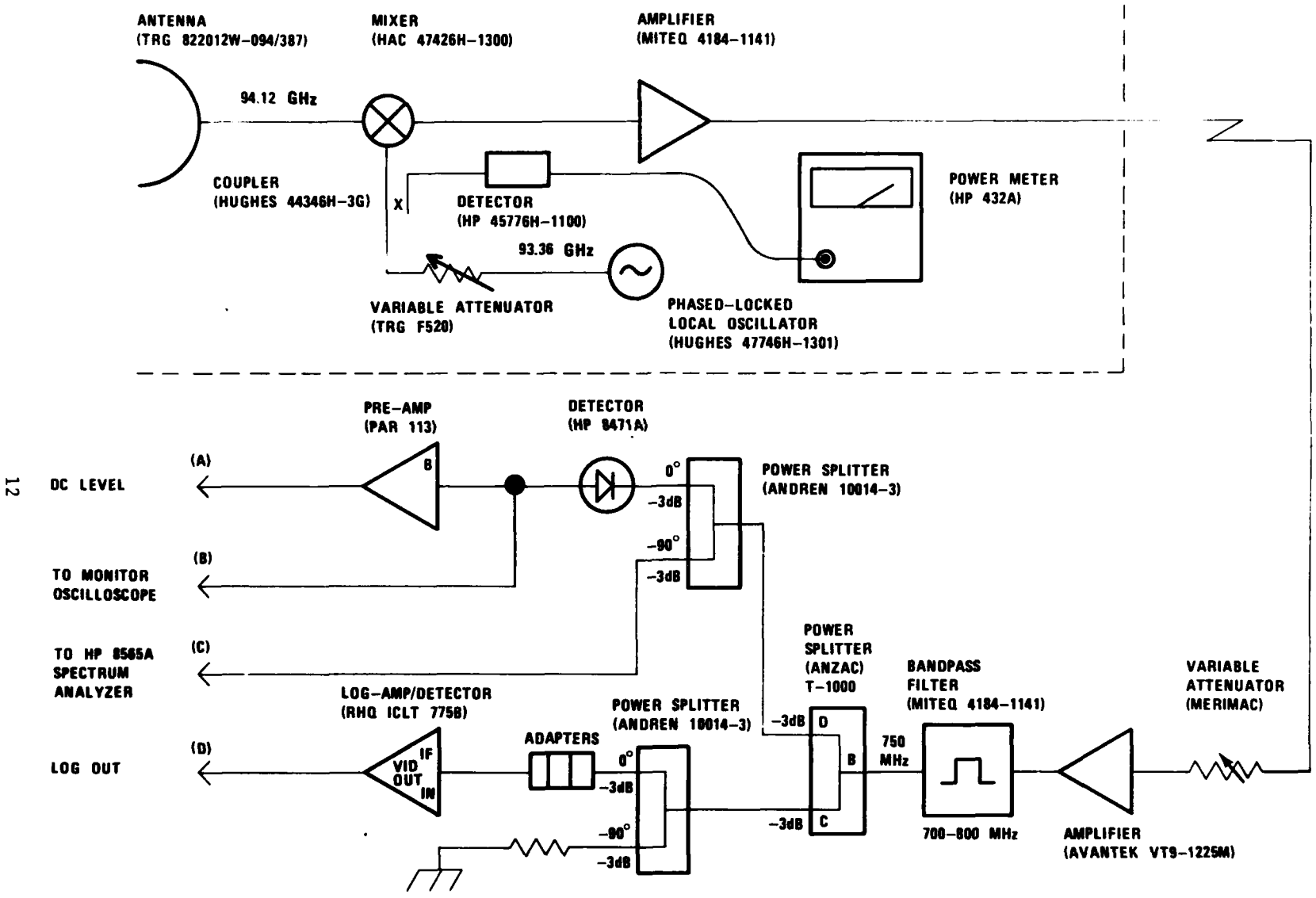

Figure 5. 94GHz receiver schematic diagram.

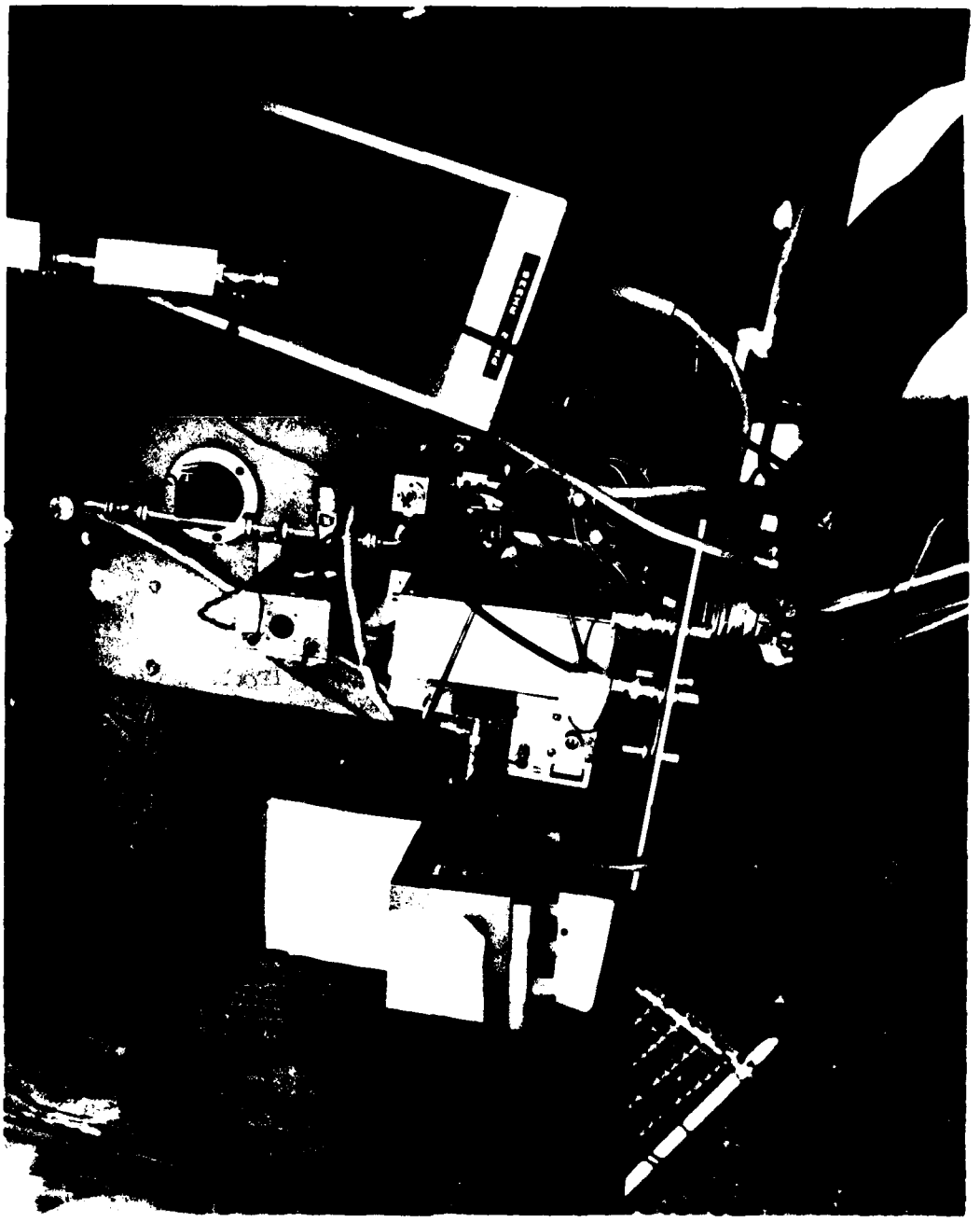

Figure 6. 94 GHz receiver front end component.

The second path of the initial power splitting led via a second power splitter and some adapters to a log-amplifier/detector. The output of this device is a dc level proportional to the logarithm of the input signal power. The output of this device was also displayed on an oscilloscope before being recorded. Figure 7 is a photograph of the IF processing layout (on top of the spectrum analyzer) as it was used for the tests. At the right is the input attenuator. At the left, painted black, is the log-amplifier/detector, and behind the circuitry is the square-law detector amplifier.

The desired atmospheric scintillation information was contained in signals from the square-law detector and the log-amplifier/detector. Each of these outputs was displayed on an oscilloscope and then directed to a lock-in amplifier used as a sensitive ac voltmeter. The output is the rms value of the ac component of the input signal. A strip-chart recorder was the primary data recording instrument for the four radar data signals, i.e., the square-law detector dc level, the square-law detector ac component, the log-amplifier/detector dc level, and the log-amplifier/detector ac component. Along with these signals, the output of the σ_χ channel of the space averaging anemometer was recorded. Figure 8 diagramatically shows the method for extracting the ac components from the signals and shows the overall data recording set-up. The actual hardware is shown in Figure 9.

It should be pointed out that the desired experimental quantity, the log-amplitude standard deviation, is not the same as the ac component of the log-amplifier/detector output. The necessary computation to obtain σ_χ is given in Appendix A.

IV. RESULTS AND ANALYSIS

The outputs of the square-law detector and the log-amplifier/detector were calibrated as a function of IF power using a signal generator at 750 MHz. These data are shown in Figures 9 and 10. Deviations from linearity are due to the difficulty in setting the input power using the spectrum analyzer.

Since, during the experiment, the attenuator in the IF chain was adjusted to give -10 dBm IF power, the calibrations were done over $\pm$20% about 0.1 mW. Following the calibration, a $\pm$5% (power) sinusoidal modulation was induced on the signal generator output. This simulated signal was used to ensure that the expected log-amplifier/detector ac voltage agreed with that seen on the ac voltmeter. This test is described in more detail in Appendix B. The outputs of the millimeter-wave system are demonstrated in Figure 11. These data were taken while a car was being driven along the road between the transmitter and receiver.

Figure 12 shows data taken 1 September, 1982 in bright sunlight with the temperature in the mid-eighties and the relative humidity between 60% and 70%. The laser log-amplitude standard deviation, σ_χ , is seen to fluctuate between 0.3 and 0.4. Taking the more conservative value of 0.3, the index-of-refraction structure parameter calculated from Equation (1) is 5.7×10^{-14} $m^{-2/3}$. C_n^2 varies from 10^{-17} $m^{-2/3}$ or less for an extremely weak turbulence to 10^{-13} $m^{-2/3}$ or more when the turbulence, generated near the ground in direct sunlight, is strong [11]. Thus, as expected, the laser system indicates a strong turbulence.

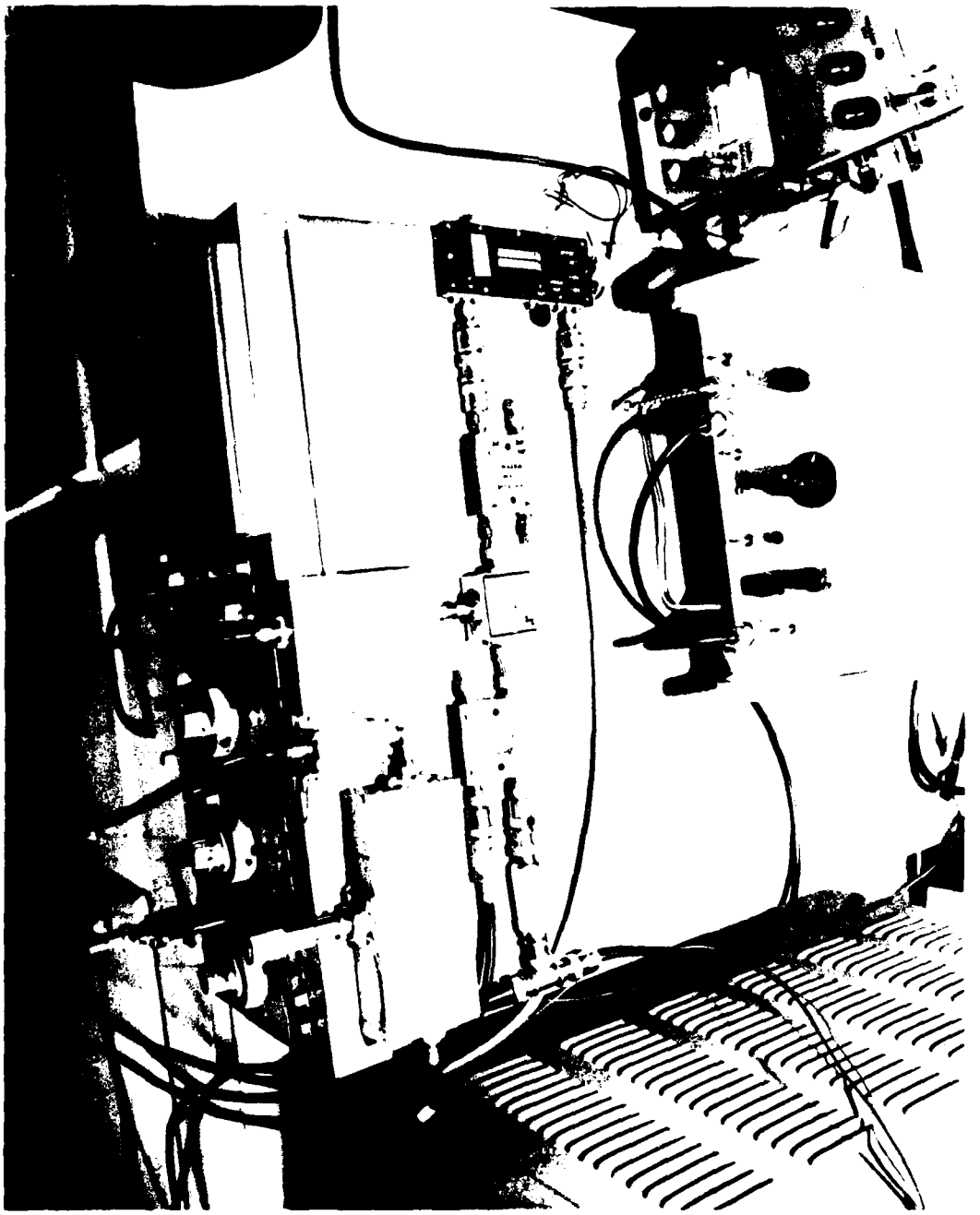

Figure 7. 94 GHz receiver IF/detector components.

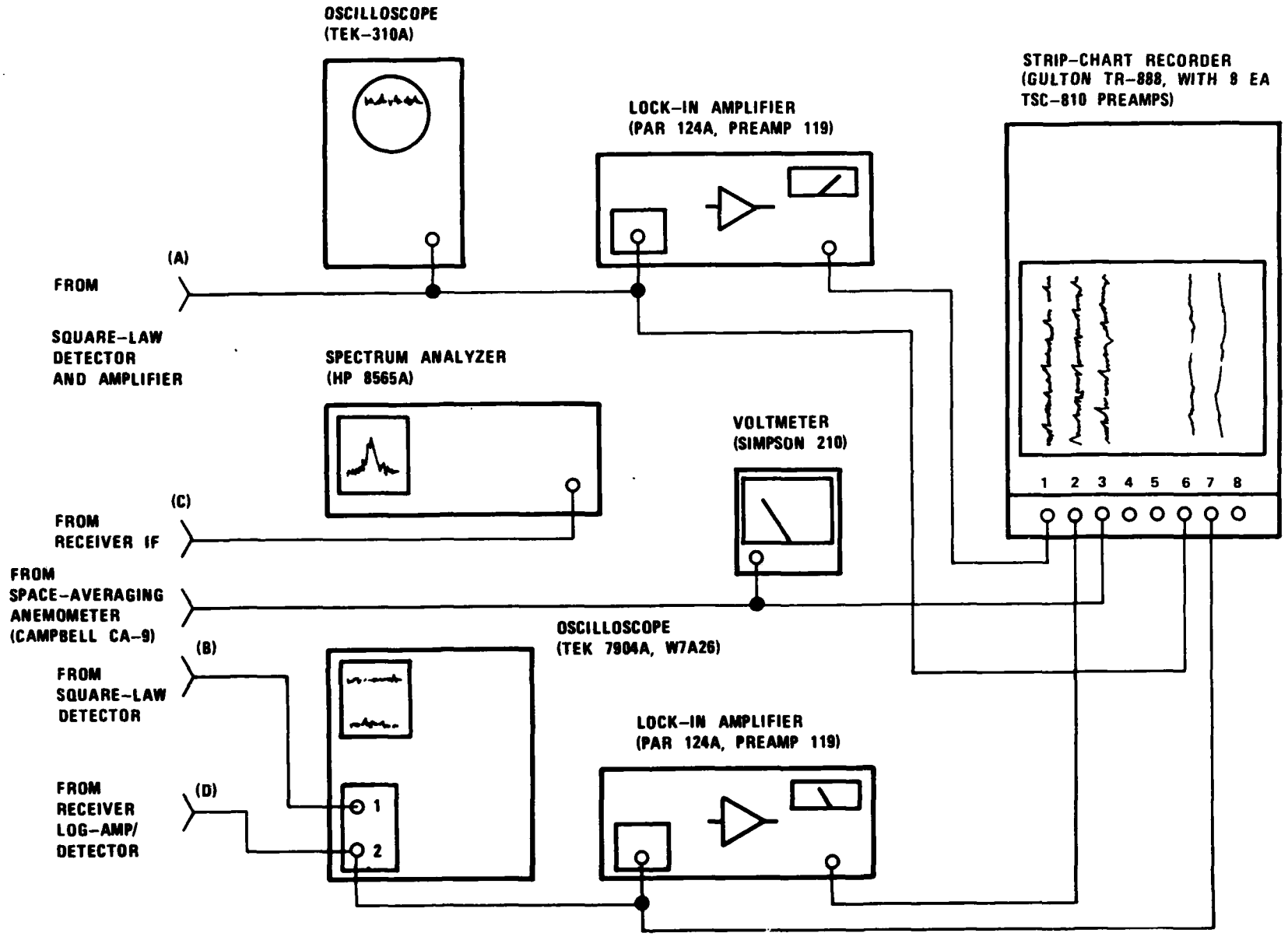

Figure 8. Data processing/recording block diagram.

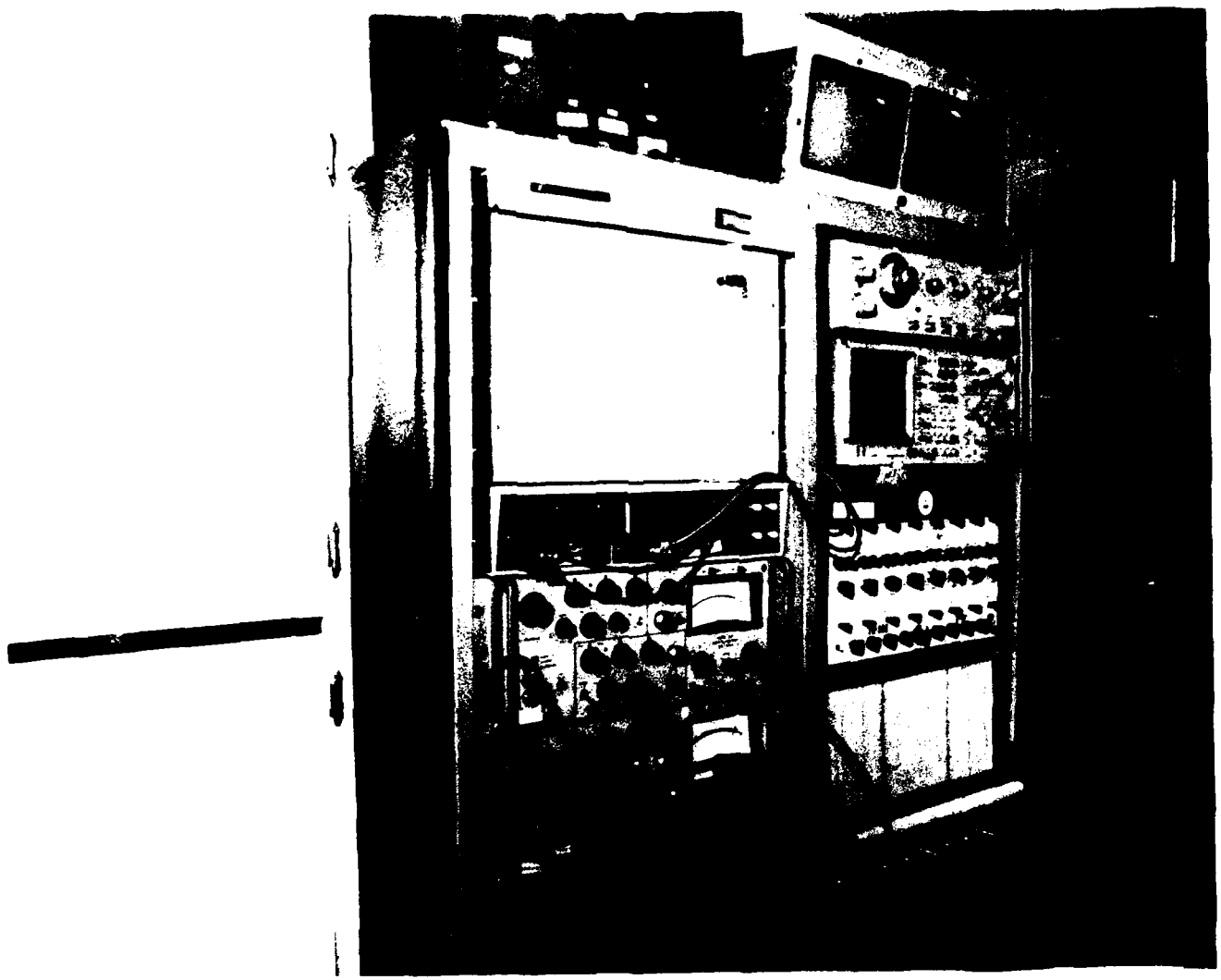

Figure 9. Data processing/recording equipment.

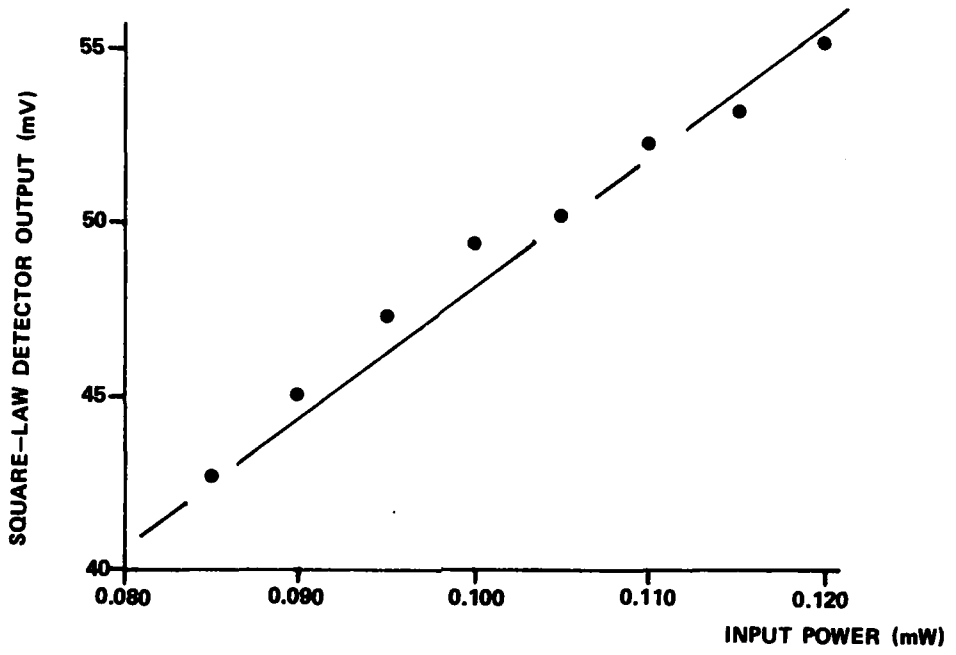

Figure 9. Square-law detector output.

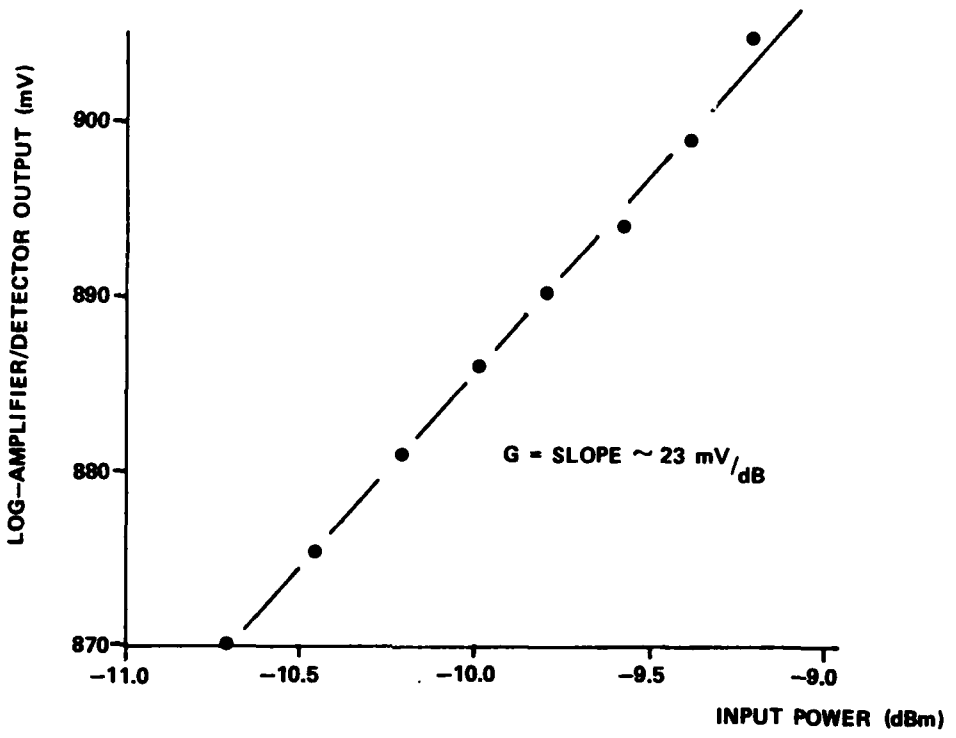

Figure 10. Log-amplifier/detector output.

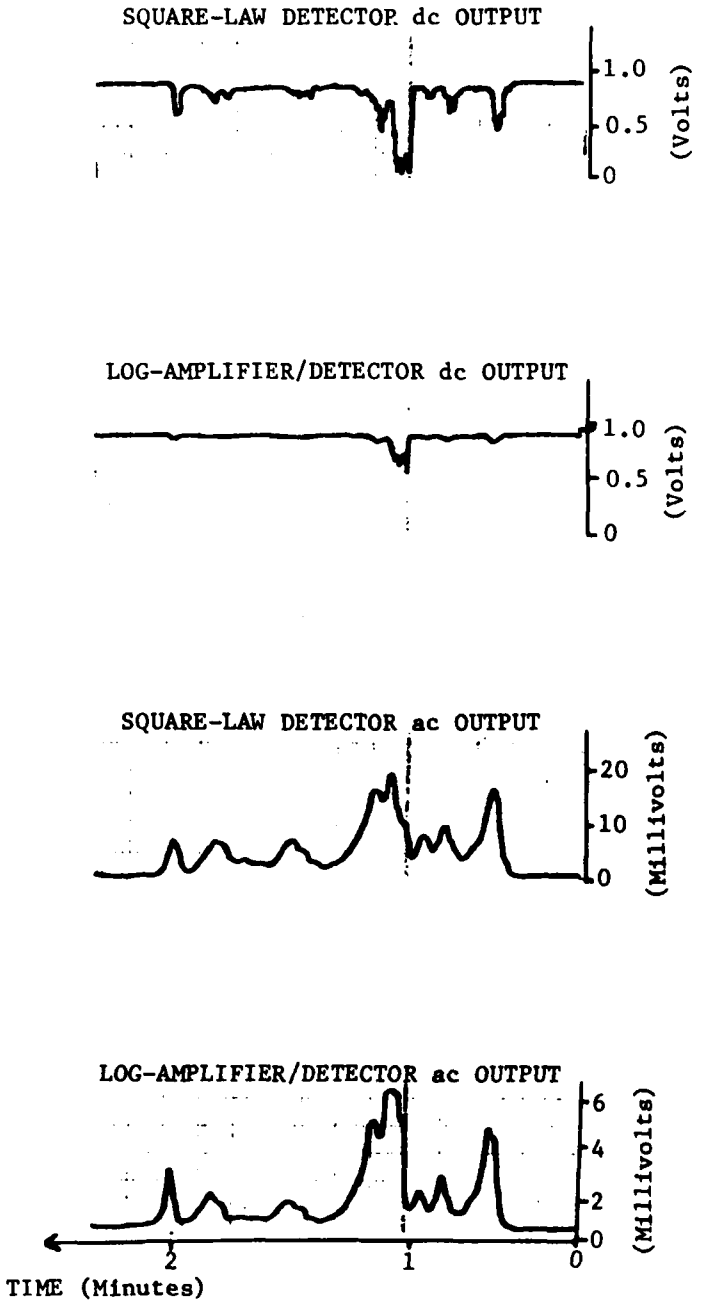

Figure 11. 94 GHz system outputs.

Using the above computed value for C_n^2, the expected σ_χ for the millimeter-wave system is determined from Equation (1) to be 7.6×10^{-3}. Using this result, Equation (A-18) gives an expected log-amplifier/detector ac output of 1.5 mV.

As can be seen from Figure 12, the output observed was generally much less, on the order of 0.3 mV, except for occasional large increases (some of which are truncated by the strip-chart recorder). However, after simultaneously monitoring these large swings and observing the IF frequency on the spectrum analyzer, it became clear that the large outputs were correlated with IF frequency jumps on the order of 10 MHz. Smaller peaks in the ac output coincided with smaller frequency jumps.

At this point, it was suspected that transmitter/receiver induced amplitude fluctuations were being observed, rather than atmospheric scintillations. The transmitter klystron was suspected despite the fact that the power output, as monitored with a Schottky-diode dectector, was very constant, showing variations of ~ 0.1% over 5 minutes. It is not clear if the amplitude modulation was due to the klystron output changing with frequency or to frequency-response characteristics of the receiver components, or both.

As a test of transmitter/receiver amplitude noise, the transmitter was coupled (with some attenuation) directly to the receiver and set for a -10 dBm IF power. The log-amplifier/detector ac output for this test is shown in Figure 13, and, as can be seen, it does not differ significantly from the scintillation test.

Thus, it must be concluded that amplitude fluctuations resulting from atmospheric scintillation are small, and probably are at least an order of magnitude smaller than the amplitude noise due to the transmitter and receiver. If it is assumed that the log-amplifier/detector ac output for atmospheric scintillations would be on the order of 0.03 mV, the corresponding log-amplitude standard deviation is $\sigma_\chi = 1.5 \times 10^{-4}$. For this experiment, then, the atmospheric scintillation for millimeter waves is about one-tenth of that predicted from Equation (1).

In retrospect, this result is not surprising, considering the assumptions invoked in the optical theory. A heuristic argument for the millimeter-wave experiment may be made: the outer scale of the turbulent eddies is small compared to the Fresnel-zone size. If L_o is taken to be about one-third the height above the ground, then, for this experiment, $L_o \sim 0.3$ m, considerably less than $\sqrt{\lambda R} \sim 2.0$ m. The turbulent-eddy sizes that contribute most to the amplitude fluctuations do not exist for the millimeter wave system. Unfortunately, no simple quantitative models have been developed for $L_o < \sqrt{\lambda R}$ [12].

It should be pointed out, however, that other workers have obtained conflicting experimental results [13,14]. Ho, et.al. (as presented in Kulpa and Brown) studied fluctuations at 110 GHz over a 4-kilometer path using 50-cm antennas about 50 m above ground. Peak values for σ_χ were ~ 2.6×10^{-2}, corresponding to $C_n^2 \sim 4 \times 10^{-14}$ $m^{-2/3}$. Lane, et.al. made measurements at 100-110 GHz over a 300-m path, 2.0 m above ground using 15-cm antennas. Their maximum fluctuations give $\sigma_\chi \sim 2.3 \times 10^{-2}$ and $C_n^2 \sim 7 \times 10^{-12}$ $m^{-2/3}$. This latter result is highly suspect since it is indicative of extremely strong turbulence.

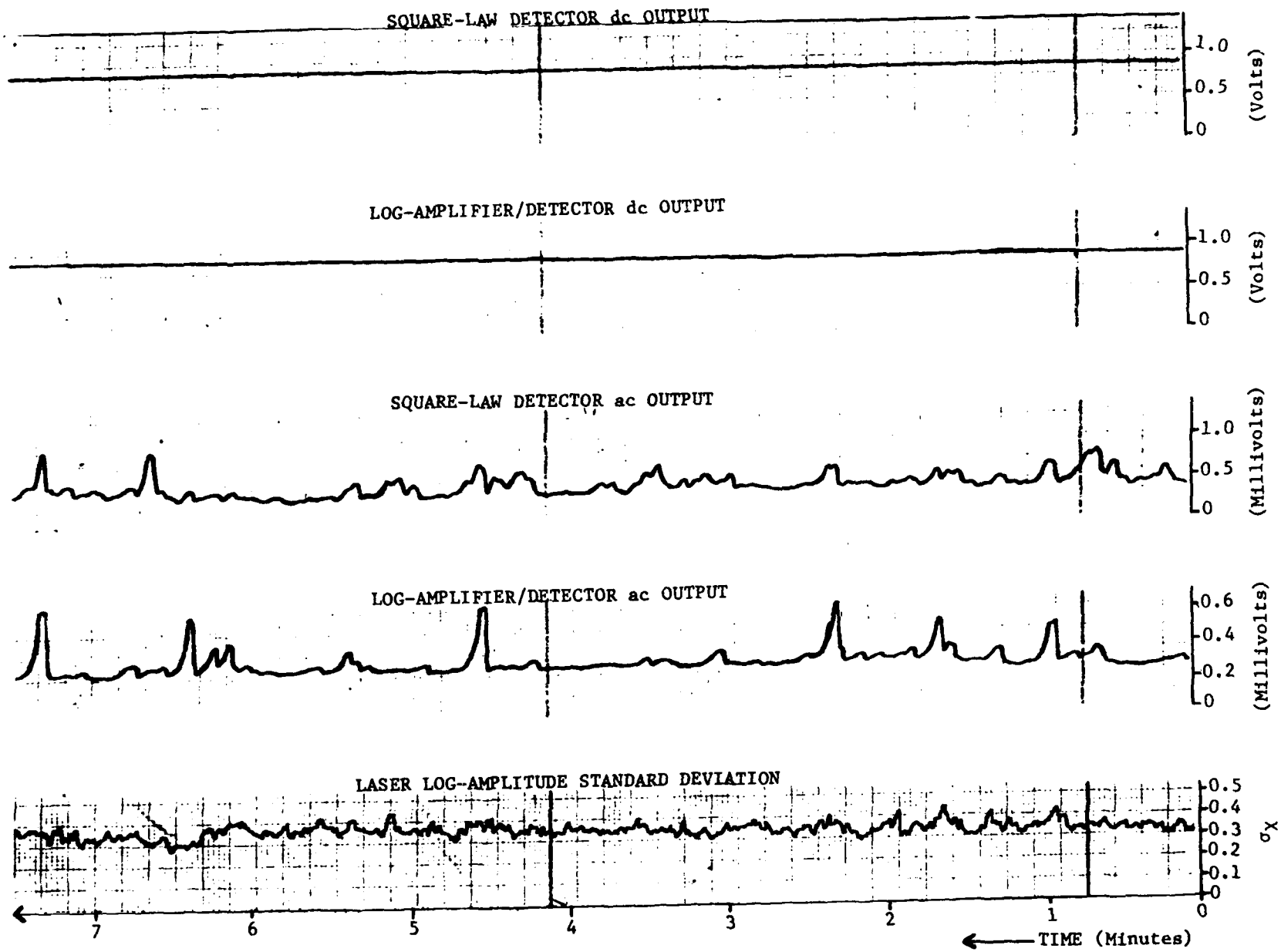

Figure 12. Atmospheric scintillation data.

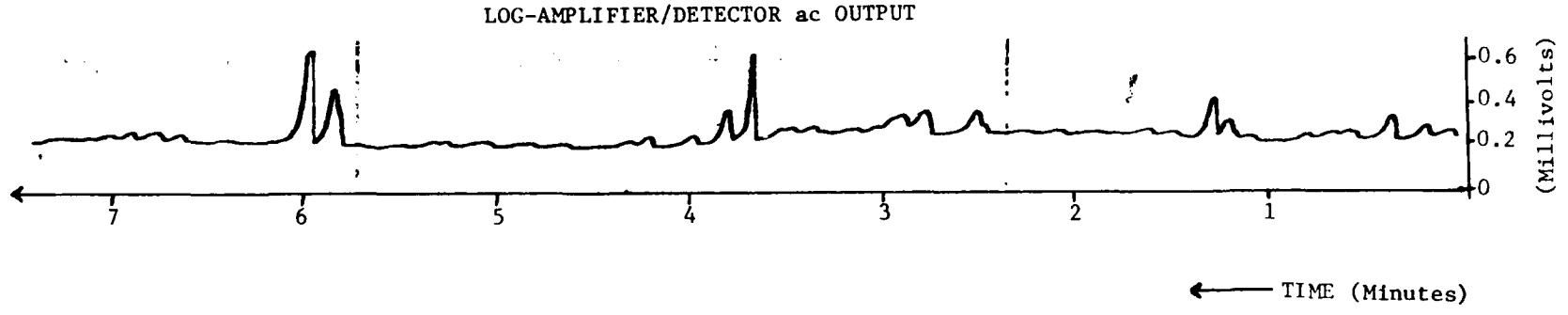

Figure 13. Transmitter/receiver amplitude noise.

As stated in the introduction, the intent of this work was to gain some insight into tracking errors in conical-scan and monopulse radars caused by clear-air turbulence. With the caveat that the theory may not apply, the mean square angle of arrival is given approximatley by [10].

$$\langle \alpha^2 \rangle \simeq \frac{3}{D^{1/3}} \int_0^R C_n^2 (x)\, dx \quad , \qquad (10)$$

where D is the aperature diameter, and $C_n^2(x)$ is integrated along the path length. If the medium is homogeneous, or if we assume some sort of average value for C_n^2, then

$$\langle \alpha^2 \rangle \simeq \frac{3 C_n^2 R}{D^{1/3}} \quad . \qquad (11)$$

For $\sigma_\chi = 1.5 \times 10^{-4}$ for millimeter waves, an "effective value" of C_n^2 computed from Equation (1) is $2.3 \times 10^{-17}\ m^{-2/3}$. Using this value for C_n^2, a range of 5 kilometers, and a 60-cm antenna,

$$\langle \alpha^2 \rangle = \frac{3\left(2.3\times10^{-17}\ m^{-2/3}\right)\left(5\times10^{3}\ m\right)}{\left(0.60 m\right)^{1/3}} \qquad (12)$$

$$= 4 \times 10^{-13}\ \text{rads}^2 \quad .$$

The rms angle fluctuation is ~ 10^{-6} rads or 1 microradian.

This figure can be related to required tracking accuracies for tactical systems in the following way. Assume that a ±1-meter accuracy at 5 kilometers is required with a 95% probability. The angle α is normally distributed with zero mean and $\sqrt{\langle \alpha^2 \rangle} = \sigma$. Then the angle accuracy required is $\pm 2\sigma$, so that

$$\pm 2\sqrt{\langle \alpha^2 \rangle} = \frac{\pm 1 \text{ meter}}{5 \text{ kilometers}} \quad ,$$

or $\sqrt{\langle \alpha^2 \rangle} = 0.1$ mrad. Thus, the angle error due to clear-atmosphere turbulence is 1% of the angular-error budget, versus ~ 30% calculated from the optically-measured C_n^2 of $5.7 \times 10^{-14}\ m^{-2/3}$.

This result, however, does not agree with other angle-of-arrival error measurements at millimeter wavelengths [16,17,18]. At 150 GHz over a 5.6 km path 10 meters above the ground (mean height), Andreyev, et.al. found rms angle fluctuations of approximately 0.1 mrad, the entire error budget. Similar results were obtained by McMillan et.al. based on angle-of-arrival calculations using experimental intensity-fluctuation data. Somewhat more encouraging results were reported by C. W. Tolbert, et.al. at 35 GHz over a 16-km path (from one mountain peak to another in Colorado) using 4° half-power

beamwidths. Measured rms angle variations ranged from too small to measure to 0.085 mrad. The variety of experimental results, both for amplitude fluctuations and angle-of-arrival errors, are probably indicative of the difficulty of making the measurements and in characterizing measurement conditions.

A heuristic argument can also be made for small angle-of-arrival errors in millimeter-wave radars close to the ground. According to Fante, [19] "...when a laser beam interacts with the turbulent eddies it is found that those eddies which are large compared to the diameter of the beam tend to deflect the beam, whereas those eddies which are small compared with the beam diameter tend to broaden the beam, but do not deflect it significantly." If the millimeter beam is considered to be bounded by a cylinder out to a distance of D^2/λ and by a cone having the nominal beamwidth beyond that point, [20] then, for an antenna aperture of 0.6 meters, the beam diameter is always considerably larger than the estimated outer scale of the turbulent eddies (0.3 m). Thus, gross angular deflections of the entire beam are expected to be small.

The argument above, however, brings out another consideration with respect to the theory. Because of the large millimeter-wave aperture, far-field (and plane-wave) conditions are met at a considerable longer range than for the laser system, by about an order of magnitude. Thus, antenna near-field effects may be considerable for millimeter measurements.

V. CONCLUSIONS

A negative result is reported for this experiment in that the amplitude fluctuations at 94 GHz due to clear-air atmospheric turbulence could not be observed above the transmitter/receiver noise. The necessity of carefully characterizing this noise is well demonstrated. It is believed that had the transmitter been a highly-stable, phase-locked source (as the local oscillator was), the atmospheric turbulence could have been measured.

Despite this negative result, it is felt that an estimated upper bound for the fluctuations was reasonably established, and that this upper bound was about a factor of ten lower than fluctuations predicted from the optical theory. There is reason to believe that angle-of-arrival fluctuations may also be smaller for millimeter-wave systems.

APPENDIX A

DETERMINATION OF σ_χ FOR MILLIMETER-WAVE SYSTEM

APPENDIX A

DETERMINATION OF σ_χ FOR MILLIMETER-WAVE SYSTEM

The millimeter-wave system used in this experiment did not measure the log-amplitude standard deviation σ_χ directly, and some careful analysis is required to compute it from the output of the system shown in Figure A1.

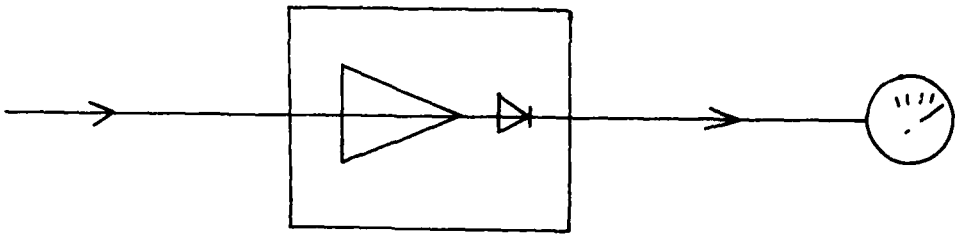

Figure A1. σ_χ measurement.

The output of the log-amplifier/detector is a voltage given by

$$V_{log}(t) = G\ 10\ \log\ \left[p(t)/p_R\right] \quad , \qquad \text{(A-1)}$$

where G is the "gain" of the amplifier in volts/dB, p(t) is the IF power, and p_R is the input power for which the output voltage V_{log} equals zero; p_R can be thought of as some internal reference used by the log-amplifier/detector. Note also from Equation (A-1) that the output is in terms of the logarithm to the base 10, rather than the logarithm to the base e as desired.

The voltage $V_{log}(t)$ is applied to the rms AC voltmeter; the output of the voltmeter V_o is equal to the standard deviation of $V_{log}(t)$,

$$V_o = \sqrt{\langle V^2_{log}(t)\rangle - \langle V_{log}(t)\rangle^2} \qquad \text{(A-2)}$$

$$= 10G \sqrt{\langle \log^2 \left[p(t)/p_R\right]\rangle - \langle \log \left[p(t)/p_R\right]\rangle^2} \qquad \text{(A-3)}$$

$$= (4.343)G \sqrt{\langle \ln^2 \left[p(t)/p_R\right]\rangle - \langle \ln \left[p(t)/p_R\right]\rangle^2} \qquad \text{(A-4)}$$

In the last step, base 10 logs are converted to natural logs using

$$10g\ x = 0.43429\ \ldots\ \ln x \quad . \qquad \text{(A-5)}$$

If we now set

$$p(t) = p_o + p_1(t) \quad , \qquad \text{(A-6)}$$

where

$$p_o = p(t) \qquad \text{(A-7)}$$

we can write

$$\ln \left[p(t)/p_R\right] = \ln \left[p_o/p_R + p_1(t)/p_R\right] \qquad \text{(A-8)}$$

$$= \ln \left[p_o/p_R \left(1 + p_1(t)/p_o\right)\right] \qquad \text{(A-9)}$$

$$= \ln \left(p_o/p_R\right) + \ln \left[1 + p_1(t)/p_o\right] \quad . \qquad \text{(A-10)}$$

If now the power fluctuations about the mean are very small (as they evidently were for this experiment), to a good approximation

$$\ln \left[p(t)/p_R\right] \simeq \ln \left(p_o/p_R\right) + p_1(t)/p_o \qquad \text{(A-11)}$$

and

$$\langle \ln \left[p(t)/p_R\right] \rangle \simeq \ln \left(p_o/p_R\right) \quad . \qquad \text{(A-12)}$$

Using this result, the quantity in the radical of Equation (A-4) becomes

$$\langle \ln^2 \left[p(t)/p_R\right] \rangle - \left(\ln p_o/p_R\right)^2 \qquad \text{(A-13)}$$

$$= \langle \left(\ln \left[p(t)/p_R\right] - \ln p_o/p_R\right)^2 \rangle \qquad \text{(A-14)}$$

$$= \langle \ln^2 \left\{\frac{\left[p(t)/p_R\right]}{p_o/p_R}\right\} \rangle = \langle \ln^2 \left[p(t)/p_o\right] \rangle \quad . \qquad \text{(A-15)}$$

This result is the log-power (log-intensity) variance,

$$\sigma^2_{lnp} \triangleq \left\langle \ln^2 \left[p(t)/p_o \right] \right\rangle \quad , \qquad \text{(A-16)}$$

and since

$$\sigma^2_{lnp} = 4\,\sigma_\chi^2 \quad ,$$

Equation (A-4) becomes

$$V_o = 4.343\ G \sqrt{4\,\sigma_\chi^2} \quad , \qquad \text{(A-17)}$$

or

$$\sigma_\chi = \frac{V_o}{2(4.343)G} \quad . \qquad \text{(A-18)}$$

APPENDIX B

MEASUREMENT SYSTEM TEST

APPENDIX B

MEASUREMENT SYSTEM TEST

In order to test that system of Figure A1, a signal generator with a small sinusoidal amplitude modulation at 40 Hz was used as a simulated IF input. In terms of the log-power variance, Equation (A-17) becomes

$$V_o = (4.343)G \sqrt{\sigma^2_{lnp}} \quad , \qquad \text{(B-1)}$$

or

$$V_o = (4.343)G \sqrt{\langle \ln^2 \left[p(t)/p_o\right]} \quad . \qquad \text{(B-2)}$$

For a sinusoidal variation

$$p(t) = p_o + p_1 \cos(wk) \quad , \qquad \text{(B-3)}$$

and

$$\sigma^2_{lnp} = \left\langle \ln^2 \left(1 + \frac{p_1}{p_o} \cos(wk)\right)\right\rangle \quad . \qquad \text{(B-4)}$$

Using the expansion

$$\ln(1 + x) = x - \frac{x^2}{2} + \frac{x^3}{3} - \cdots \quad , \qquad \text{(B-5)}$$

an approximation for $p_1/p_o << 1$ gives

$$\sigma^2_{lnp} \simeq \left\langle \left(\frac{p_1}{p_o}\right) \cos(wk)^2 \right\rangle \qquad \text{(B-6)}$$

$$= \left(\frac{p_1}{p_o}\right)^2 \langle \cos^2 wk \rangle \qquad \text{(B-7)}$$

$$= \frac{1}{2} \left(\frac{p_1}{p_o}\right)^2 \qquad \text{(B-8)}$$

Using this result in Equation (B-1) gives

$$V_o \simeq \frac{(4.343)G}{\sqrt{2}} \left(\frac{p_1}{p_c}\right) \quad . \qquad \text{(B-9)}$$

For the system test, the IF power was set to oscillate about 0.1 mW (-10 dBm) from 0.095 mW to 0.105 mW. This oscillation was actually set by observing the square-law detected output on an oscilloscope and using the calibration data of Figure 9.

From Equation (B-9), the expected ac voltmeter output is

$$V_o = \frac{(4.343)(23\ \text{mV/dB})}{\sqrt{2}} \left(\frac{0.005\ \text{mW}}{0.100\ \text{mW}}\right)$$

$$= 3.5\ \text{mW}.$$

The output of the ac voltmeter was actually 3.2 mV, a very reasonable agreement considering the uncertainties involved in setting the amplitude modulation and the approximations made.

ADDENDUM

In a more recent review article by Fante [21], the index of refraction structure parameter for millimeter waves is discussed. In particular, for the case where the outer scale of turbulent eddies, L_o, is smaller then the first Fresnel-zone size, $\sqrt{\lambda R}$ (~ 2 meters for this experiment), the equation

$$\sigma_\chi^2 \simeq \frac{1}{2} K^2 C_n^2 L_o^{5/3} R$$

is more applicable than Equation (1) (for weak turbulence). Assuming the following millimeter wave values for this experiment,

$\sigma_\chi = 1.5 \times 10^{-4}$
$L_o = 0.3$ meters
$R = 1,232$ meters
$k = 2\pi/\lambda$, $\lambda = 3.19$mm

the value for C_n^2 calculated from the above equation is 2.2×10^{-16} $m^{-2/3}$. This value is about an order of magnitude larger than the "effective value" of C_n^2 computed from Equation (1) (2.3×10^{-17} $m^{-2/3}$), and, consequently, the rms angle-of-arrival error computed from Equation (12) is increased by about a factor of three. This is not a significant change, compared to estimates of $\sqrt{\langle \alpha^2 \rangle}$ of one millimeter.

Recent theoretical efforts at the US Army Missile Command also support the notion that angle-of-arrival errors are significantly larger than measured values of σ_χ would indicate [22]. The model uses measured millimeter data for the temperature structure coefficient, the water vapor structure coefficient, and their cross-correlation to compute C_n^2, σ_χ, and $\sqrt{\langle \alpha^2 \rangle}$. For a strong turbulence, high humidity, and strong wind speed, computed values for σ_χ were 2×10^{-4} to 8×10^{-4}, which is in reasonable agreement with the result from this experiment. The wind speed is an important factor in the model; the experiment was performed on very calm days.

The angle-of-arrival errors predicted by the model are generally larger than one milliradian with the power spectral density largely below 5 Hz. Thus, there is a good deal of evidence to indicate that very significant tracking errors in millimeter wave radar will be due to clear-air turbulence. Further work in this area is now being supported by the Army Research Office, [23] and it is hoped that definitive measurements will result.

REFERENCES

1. Tatarski, V. I., Wave Propagation in a Turbulent Medium, translated from the Russian by R. A. Silverman, New York, McGraw-Hill Book Company, Inc., 1961.

2. Lawrence, R. S. and J. W. Strohbehn, "A Survey of Clear-Air Propagation Effects Relevant to Optical Communications," Proc. IEEE, Vol. 58, No. 10, October 1970, pp. 1523-1545.

3. Fante, R. L., "Electromagnetic Beam Propagation in Turbulent Media," Proc. IEEE, Vol. 63, No. 12, December 1975, pp. 1669-1692.

4. McMillan, R. W., R. A. Bohlander, and G. R. Ochs, "Instrumentation for Millimeter Wave Turbulence Measurements," Proc. SPIE Conf. on Atmospheric Effects on Electro-Optical, Infrared, and Millimeter Wave Systems Performance, August 27-28, 1981, San Diego, CA.

5. Etcheverry, R. D., G. R. Heidbreder, W. A. Johnson, and H. J. Wintroub, "Measurements of Spatial Coherence in 3.2-mm Horizontal Transmission," IEEE Trans. Antennas Propagation, Vol. AP-15, No. 1, January 1967, pp. 136-141.

6. Tatarski, V. I., Reference 1, p. 153.

7. Tatarski, V. I., Reference 1, p. 140.

8. Skolnik, M. I., Introduction to Radar Systems, 2nd Ed., New York, McGraw-Hill Book Company, 1980, Chapter 13, p. 511.

9. Lawrence, R. S., et.al., Reference 2, p. 1529.

10. Lawrence, R. S., G. R. Ochs, and S. F. Clifford, "Use of Scintillations to Measure Average Wind Across a Light Beam," Applied Optics, Vol. 11, No. 2, February 1972, pp. 239-243.

11. Lawrence, R. S., et.al., Reference 2, p. 1526.

12. Kulpa, S. M. and E. A. Brown, "Chapter I. -Introduction and Overview," in Near-Millimeter Wave Technology Base Study, S. M. Kulpa and E. A. Brown, ed., Volume I - Propagation and Target/Background Characteristics, Report Number HDL-SR-79-8, November 1979, p. 20.

13. Kulp, A. M., et.al., Reference 12, p. 23.

14. Lane, J. A., A. C. Gordon-Smith, and A. M. Zavody, "Absorption and Scintillation Effects at 3 mm Wavelength on a Short Line-of-Sight Radio Link," Electronic Letters, Vol. 3, No. 5, May 1967, pp. 185-186.

15. Fante, R. L., Reference 3, p. 1681.

16. Andreyev, V. A., V. A. Golunov, A. T. Ismailov, A. A. Parshikov, B. A. Rozanov, and A. A. Tanyigin, "Intensity and Angle of Arrival Fluctuations of Millimetric Radiowave in Turbulent Atomsphere," Joint Anglo-Soviet Seminar on Atmospheric Propagation at Millimeter Wavelengths, Moscow, Nov 28 - Dec 3, 1977, pp. R1-8.

17. McMillan, R. W., R. A. Bohlander, D. G. Bauerle, G. R. Ochs, R. J. Hill, S. F. Clifford, and J. Nemarich, "Millimeter Wave Atmospheric Turbulence Measurements: Preliminary Results," Proceedings of the SPIE, Vol. 337, Millimeter Wave Technology, August 1982.

18. Tolbert, C. W., B. M. Fannin, and A. W. Straiton, Amplitude and Phase Difference Fluctuations of 8.6 Millimeter and 3.2 Centimeter Radio Waves on Line-of-Sight Paths, Electrical Engineering Research Laboratory, University of Texas, Report 78, 16 Mar 56, (DDC AD 08810).

19. Fante, R. L., Reference 2, p. 1673.

20. Spencer, N. A., "Factors in Antenna Design," in Moder Radar, R. S. R. S. Berkowitz, ed., New York, John Wiley & Sons, Inc., 1965, Part V, Ch. 2, p. 385.

21. Fante, R. L., "Electromagnetic Beam Propagation in Turbulent Media: An Update," Proc. IEEE, Vol. 68, No. 11, November 1980, pp. 1424-1443.

22. Private Communication, H. F. Anderson, US Army Missile Laboratory, Redstone Arsenal, AL, January 1983.

23. McMillan, R. W. and R. A. Bohlander (Georgia Institute of Technology, Engineering Experiment Station, Atlanta, GA) and G. R. Ochs, R. J. Hill, and S. F. Clifford (National Oceanic and Atmospheric Administration, Environmental Research Laboratories, Wave Propagation Laboratory, Boulder, CO), "Millimeter Wave Atmospheric Turbulence Measurements: Preliminary Results and Instrumentation for Future Measurements," Report Draft, received December 1982.

DISTRIBUTION LIST

	COPIES
IIT Research Institute Guidance and Control Information and Analysis Center (GACIAC) 10 West 35th Street Chicago, IL 60616	1
Commander US Army Material Systems Analysis Activity ATTN: DRXSY-MP Aberdeen Proving Ground, MD 21005	1
Commander US Materiel Development and Readiness Command 5001 Eisenhower Avenue Alexandria, VA 22333	1
Commander Defense Advanced Research Projects Agency 1400 Wilson Boulevard Arlington, VA 22209	1
Commander US Army Research Office PO Box 12211 Research Triangle Park, NC 27709	1
Commander US Army Armament R&D Command Picatinny Arsenal, Dover, NJ 07801	1
Commander US Army Armament R&D Command Ballistic Research Laboratories Aberdeen Proving Ground, MD 21005	1
Commander US Army Aviation R&D Command PO Box 209 St. Louis, M. 63166	1
Commander US Army Electronics R&D Command Atmospheric Sciences Laboratory White Sands Missile Range, NM 88002	1
Commander US Army Electronics R&D Command US Army Electronic Warfare Laboratory Ft. Monmouth, NJ 07703	1

	COPIES
Commander US Army Electronics R&D Command Office of Missile Electronic Warfare White Sands Missile Range, NM 88022	1
Commander US Army Electronics R&D Command Combat Surveillance and Target Acquisition Laboratory Ft. Monmouth, NJ 07703	1
Commander US Army Electronics R&D Command Electronic Warfare Laboratory Ft. Monmouth, NJ 07703	1
Commander US Army Electronics R&D Command Electronics Technology and Devices Laboratory Ft. Monmouth, NJ 07703	1
Commander US Army Electronics R&D Command Night Vision and Electro-Optics Laboratory Ft. Belvoir, VA 22060	1
Commander US Army Electronics R&D Command Harry Diamond Laboratories 2800 Powder Mill Road Adelphi, MD 20783	1
Commander US Army Electronics R&D Command Project Manager, SOTAS Ft. Monmouth, NJ 07703	1
Commander US Army Mobility Equipment R&D Command Ft. Belvoir, VA 22060	1
Commander US Army Air Mobility Research and Development Laboratory AMES Research Center Moffett Field, CA 94035	1
Commander US Army Tank-Automotive Command Warren, MI 48090	1

	COPIES
Commander US Army Missile Command Ballistic Missile Defense Advanced Technology Center PO Box 1500 Huntsville, AL 35807	1
Commander US Naval Research Laboratory ATTN: Code 5300, Radar Division Washington, DC 20390	1
Commander US Naval Air Development Center Sensors & Avionics Technology Directorate Radar Division/Tactical Radar Branch Warminster, PA 18974	1
Commander US Naval Electronics Laboratory Center San Diego, CA 92152	1
Commander US Naval Surface Weapons Center Dahlgren, VA 22448	1
Commander US Naval Surface Weapons Center White Oak Laboratory Silver Spring, MD 20910	1
Commander US Naval Weapons Center China Lake, CA 93555	1
Commander US Air Force Systems Command US Air Force Armament Laboratory Eglin Air Force Base, FL 32542	1
Commander US Air Force Systems Command US Air Force Avionics Laboratory Wright-Patterson Air Force Base, OH 45433	1
Commander US Air Force Systems Command Air Force Cambridge Research Laboratories Hanscom Air Force Base, MA 01731	1

	COPIES
Commander US Air Force Systems Command Rome Air Development Center Griffiss Air Force Base, NJ 13441	1
Director Defense Advanced Research Projects Agency 1400 Wilson Boulevard Arlington, VA 22209	1
Director Division 8 MIT Lincoln Laboratory Lexington, MA 02173	1
Director Radar and Instrumentation Laboratory Engineering Experiment Station Georgia Institute of Technology Atlanta, GA 30332	1
Automation Industries, Inc. Vitro Laboratories Division 14000 Georgia Avenue Silver Spring, MD 20910	1
Aerojet Electro Systems 1100 W. Hollyvale Street P.O. Box 296 Azusa, CA 91702	1
AIL Division Cutler-Hammer Deer Park Long Island, NY 11729	1
AVCO Systems Division 201 Lowell Street Wilmington, MA 01887	1
Bell Aerospace Textron, Inc. PO Box 1 Buffalo, NY 14240	1
Bendix Mishawaka Operations 400 South Beiger Street Mishawaka, IN 46544	1

	COPIES
Boeing Aerospace Company PO Box 1470 Huntsville, AL 35807	1
Boeing Aerospace Company PO Box 3999 Seattle, WA 98124	1
Emerson Electric Company Electronics and Space Division 8100 W. Florissant Avenue St. Louis, MO 63136	1
Environmental Research Institute of Michigan Radar and Optics Division PO Box 618 Ann Arbor, MI 41807	1
Ford Aerospace & Communications Corporation Aeronutronics Division Ford Road Newport Beach, CA 92663	1
General Dynamics Pomona Division PO Box 2507 Pomona, CA 91769	1
Goodyear Aerospace Corporation 1210 Massillon Road Akron, OH 44315	1
Goodyear Aerospace Corporation Arizona Division Litchfield Park, AZ 85340	1
Lockheed Missile & Space Company, Inc. 4800 Bradford Drive Huntsville, AL 35807	1
Honeywell, Inc. Defense Systems Division 600 Second Street NE Hopkins, MN 55343	1
Hughes Aircraft Corporation Advanced Missile Systems Division Canoga Park, CA 91304	1

	COPIES
IBM Army Missile Programs Federal Systems Division Owego Tioga County, NY 13827	1
Intergraph Corporation PO Box 5183 Huntsville, AL 35805	1
Mark Resources Incorporated 4676 Admiralty Way Suite 303 Marina Del Rey, CA 90291	1
Martin Marietta Aerospace PO Box 6167 Huntsville, AL 35806	1
McDonnell Douglas Astronautics Company 3322 South Memorial Parkway, Suite 122 Huntsville, AL 35801	1
MITRE Corporation 4305 Middlesex Turnpike Bedford, MA 01730	1
Norden Systems, Inc. 314 Norden Place Norwalk, CT 06856	1
Northrop Corporation Defense Systems Division 600 Hicks Road Rolling Meadows, IL 60008	1
Raytheon Company Equipment Development Laboratories 430 Boston Post Road Wayland, MA 01778	1
RCA Government and Commercial Systems 3322 S. Memorial Parkway Suite 41 Huntsville, AL 35801	1
Riverside Research Institute 80 West End Avenue New York, NY 10023	1

	COPIES
Rockwell International Missile Systems Division 3370 Miraloma Avenue PO Box 4182 Anaheim, CA 92803	1
Singer Kearfott Division 150 Totowa Road Wayne, NJ 07470	1
Sperry Microwave Electronics PO Box 4648 Clearwater, FL 33518	1
Sperry Research Center 100 North Road Sudbury, MA 01776	1
SRI International 1611 North Kent Street Rosslyn Plaza Arlington, VA 22209	1
Technology Service Corporation 2811 Wilshire Blvd Santa Monica, CA 90403	1
Teledyne Brown Engineering Cummings Research Park Huntsville, AL 35807	1
Teledyne Micronetics 7155 Mission Gorge Road San Diego, CA 92120	1
Texas Instruments, Incorporated ATTN: Advanced Weapons Program Mail Stop 373 PO Box 405 Lewisville, TX 75067	1
TRW Defense and Space Systems Group 303 Williams Avenue, Suite 1231 Huntsville, AL 35801	1
Westinghouse Electric Corporation P.O. Box 1693 Baltimore, MD 21203	1

	COPIES
Commander US Army Electronics R&D Command ATTN: DELET-M, Mr. N. Wilson DELCS-R, Mr. D. Foiani Mr. W. Fishbein Mr. W. Johnson Ft. Monmouth, NJ 07703	 1 1 1 1
Commander US Air Force Systems Command US Air Force Armament Laboratory/DLMT ATTN: Max E. McCurry Eglin Air Force Base, FL 32542	 1
Emerson Electric Company Electronics and Space Division ATTN: Mr. R. Hermann 8100 W. Florissant St. Louis, MO 63136	 1
General Dynamics Pomona Division ATTN: Dr. H. P. Schmid 1675 W. Mission Blvd. PO Box 2507 Pomona, CA 91769	 1
Georgia Institute of Technology Engineering Experiment Station ATTN: Dr. Jim Echard Mr. Neil Alexander Dr. Clark Butterworth Mr. Charles Brown Atlanta, GA 30332	 1 1 1 1
MIT Lincoln Laboratory Division 8 ATTN: Dr. Jerry Waldman Lexington, MA 02173	 1
Rockwell International ATTN: Mr. J. J. Justus PO Box 4182 Anaheim, CA 92803	 1
Singer Kearfott Division ATTN: Mr. Robert Slater 150 Totowa Road Wayne, NJ 07470	 1

	COPIES
Sperry Research Center ATTN: Mr. Rick Barnes 100 North Road Sudbury, MA 01776	1
Systems Control Technology, Inc. ATTN: D. E. Bowyer PO Box 156 Shalimar, FL 32579	1
Commander Naval Weapons Center ATTN: Dr. Jim Battles, Code 3814 China Lake, CA 93555	1
DRSMI-R, Dr. McCorkle	1
DRSMI-R, COL Dombrowski	1
DRSMI-R, Dr. Rhoades	1
DRSMI-R, Mr. Black	1
DRSMI-RN, Dr. Dobbins	1
DRSMI-RE, Mr. Lindberg	1
DRSMI-RE, Mr. Todd	1
DRSMI-RE, Mr. Pittman	1
DRSMI-REM, Mr.Haraway	1
DRSMI-REO, Mr. Ducote	1
DRSMI-RER, Mr. Low	1
DRSMI-RES, Mr. Hatcher	1
DRSMI-REG, Mr. Root	1
DRSMI-REI, Mr. Holter	1
DRSMI-REL, Mr. Mangus	1
DRSMI-REL, Dr. Emmons	1
DRSMI-REL, Mr. Green	1
DRSMI-REL, Dr. Alexander	25
DRSMI-REL, Mr. Barley	1
DRSMI-REL, Mr. Grass	1
DRSMI-REL, Mr. Mullins	1
DRSMI-REL, Mr. Rast	1
DRSMI-RR, Dr.Hartman	1
DRSMI-RPR, RSIC	15
DRSMI-RPT, Record Set	1
DRSMI-LP, Mr. Voight	1